molecules

MDPI

Article

Microhydration and the Enhanced Acidity of Free Radicals

John C. Walton

EaStCHEM School of Chemistry, University of St. Andrews, St. Andrews KY16 9ST, UK; jcw@st-andrews.ac.uk; Tel.: +44-(0)1334-463864

Received: 31 January 2018; Accepted: 14 February 2018; Published: 14 February 2018

Abstract: Recent theoretical research employing a continuum solvent model predicted that radical centers would enhance the acidity (RED-shift) of certain proton-donor molecules. Microhydration studies employing a DFT method are reported here with the aim of establishing the effect of the solvent micro-structure on the acidity of radicals with and without RED-shifts. Microhydration cluster structures were obtained for carboxyl, carboxy-ethynyl, carboxy-methyl, and hydroperoxyl radicals. The numbers of water molecules needed to induce spontaneous ionization were determined. The hydration clusters formed primarily round the CO_2 units of the carboxylate-containing radicals. Only 4 or 5 water molecules were needed to induce ionization of carboxyl and carboxy-ethynyl radicals, thus corroborating their large RED-shifts.

Keywords: free radicals; acidity; DFT computations; hydration

1. Introduction

A transient-free radical is necessarily reactive at the site (X) of its unpaired electron (upe). In addition, a free radical with a structure containing a proton donor group may undergo ionic dissociation to a radical anion and a proton:

$$^{\bullet}XH_2WAH \rightarrow {}^{\bullet}XH_2WA^{-} + H^{+}$$

in which W is a connector or spacer group, and A is the site of the departing proton. Effectively, the free radicals in this category can function as Brφnsted acids. More than 40 years ago, Hayon and Simic drew attention to the fact that free radicals could be more acidic than parent compounds [1]. Other pulse radiologists, particularly Steenken and co-workers, demonstrated analogous behavior for the radical cations of phenols and nucleosides [2,3]. Recently, several situations have been recognized in which the radical enhancement of proton dissociations has been of key importance. For example, Buckel, Zipse, and co-workers identified facile deprotonation of a β-keto-alkyl radical as the key step in an enzyme catalyzed dehydration of (*R*)-2-hydroxyglutaryl-CoA [4,5]. A similar key step was proposed in the analogous enzyme-catalyzed dehydration of (*R*)-2-hydroxy-4-methylpentanoyl-CoA [6]. Cyclohexadienyl type radicals are intermediates in numerous base-promoted homolytic aromatic substitution (BHAS) reactions; Studer and Curran have pinpointed their enhanced acidity as the driving force for these processes [7]. In addition, Radom and co-workers have published theoretical studies showing that, in general, CH_2WOH radicals are more acidic than their parent CH_3WOH alcohols [8,9].

A recent theoretical investigation of radicals containing carboxylic acid groups gave guidance as to what structural features are required for proton loss to be enhanced. The size of the effect and the identity of the connector groups that do and do not transmit the enhancement were also studied [10]. The term "RED-shift" was adopted as a short and convenient acronym for the phenomenon of Radical Enhancement of Dissociation. Appreciable RED-shifts were shown to occur for radicals dissociating to

conjugate radical anions that allowed the displacement of an electronic charge away from their formal anionic centers coupled with displacement of spin density away from their formal radical centers.

A convenient measure of the RED-shift was found to be:

$$\Delta pK_a = pK_a(\text{model}) - pK_a(\text{radical}) \quad (1)$$

in which the models [HXH_2WAH] were structurally identical to the radicals [$^{\bullet}XH_2WAH$], except that the unpaired electrons had been replaced by -*H*-atoms.

The transient nature of most free radicals makes experimental determination of their pK_a values difficult. Consequently, comparatively few radical acid dissociation constants have been measured, and error limits are necessarily high. Fortunately, computational methods for estimating pK_as have been developed, and some of these refer directly to carboxylic acids [11–16]. These QM methods usually rely on computation of the free energies of deprotonation $\Delta G_{A\text{-}HA}$ and, with this intent, a DFT functional suitable for C-centered free radicals was developed [17]. This method enabled several radicals that had large ΔpK_a values to be pinpointed [10,18]. In this DFT method, the solvent (water) was allowed for simply by means of the CPCM continuum model [19]. A real possibility is that continuum solvent models would not be reliable for small and strong acids. Specific interactions of the solvent with the conjugate radical anions seem particularly likely because of their high charge densities. It is known that strong mineral acids spontaneously ionize in association with just a few microsolvating water molecules. For instance, both experiment and DFT computations showed that HCl dissociated into $Cl^-(H_2O)_3(H_3O^+)$ upon association with just four water molecules [20], and similar behavior was observed for other strong acids [21]. In fact, it has been noted that as the acidity of an acid increases, so the number of water molecules required to induce ionization ($N_G{}^i$) tends to decrease [17,22].

Theoretical studies of the microhydration of acids are challenging because the number of possible 3D arrays increases steeply as the number of water molecules increases. The potential energy surfaces (PES) rapidly become complex with many shallow minima. Distinguishing the global minimum from nearby local minima becomes problematic. Microhydration studies of transient acid radicals have been published for the bicarbonate radical **4H** [17] and the hydroperoxyl radical **5H** [23] (see Scheme 1). Some recent studies have shown that the limitations of the continuum models can be overcome with microhydration. For example, Close and Wardman studied di-hydration of the tyrosyl radical and discussed related structures [24]. The objectives of the present computational study were to investigate the effect microhydration has on the enhancement of acidity observed for specific free radicals with and without RED-shifts. Are the increased acidities computed with the continuum solvent model real? What effect does the upe in the radical have on the solvent microstructure? Can the number of water molecules needed to induce ionic dissociation ($N_G{}^i$) be determined for RED-shifted radicals?

2. Results and Discussion

A set of acid radicals with particular structural features was chosen for microhydration study and is shown in Scheme 1, together with experimental and computed pK_a and ΔpK_a values [10]. Three of the set contain carboxylic acid functional groups with differing spacer units. The carboxyl radicals **1Hc** & **1Ht** are very strong acids with large RED-shifts (ΔpK_a = 3.9 & 3.2, respectively), and contain the upe *formally* right on the carboxylate *C*-atom. In carboxy-ethynyl radical anion **2,** the upe and negative charge are *formally* separated by an ethynyl unit, which proved to be a very efficient conductor of RED-shift. In carboxy-methyl radical anion **3,** the upe and negative charge are *formally* separated by a methylene unit that completely negated RED-shift. The set also contains the bicarbonate radical anion **4** that has the upe and carboxylic acid group *formally* separated by an *O*-atom. The final member, hydroperoxyl **5H**, has a unique structure such that the upe and charge are *formally* on adjacent *O*-atoms. The ease of deprotonation of the acid radicals will be strongly influenced by solvation, which will stabilize the conjugate radical anions produced during dissociation more than the neutral radical precursors.

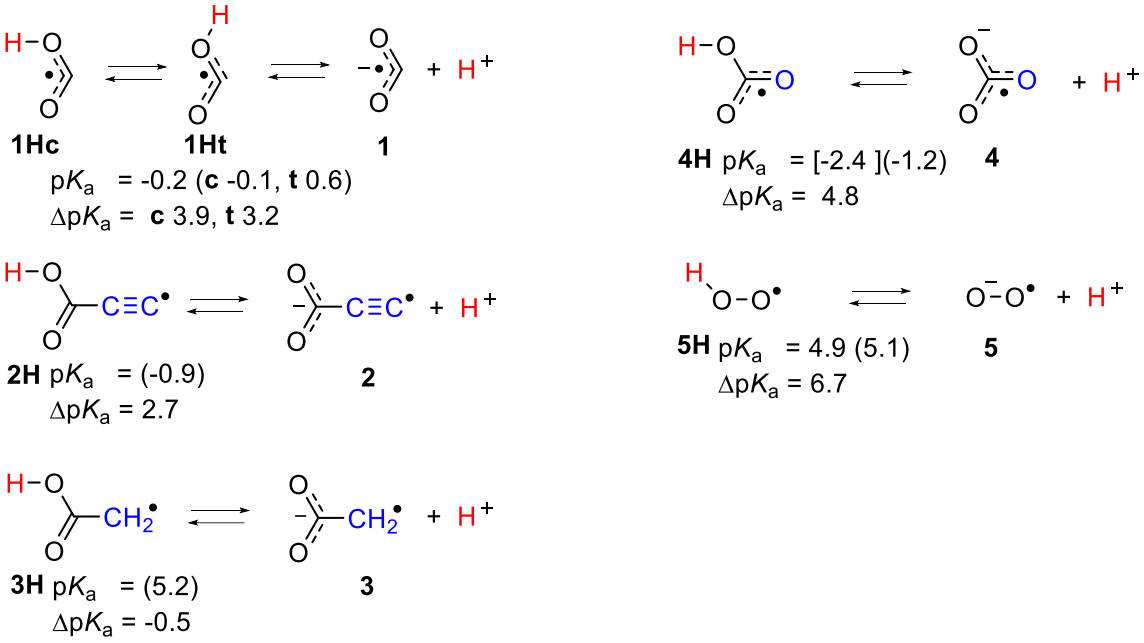

Scheme 1. Set of Acid Radicals for Microhydration Study. Experimental pK_a values with DFT computed values in parenthesis.

A benchmarking study involved comparison of 12 radical reaction types and 23 different DFT functionals (plus the MP2 ab-initio method), with the high level composite ab initio G4 method [25]. The CAM-B3LYP functional incorporating the Coulomb-attenuating method [26] gave lowest mean absolute deviations (MAD) and performed best with radical species [17]. Microhydration of the bicarbonate radical **4H,** which has a large RED-shift, was investigated using this approach; cluster configurations were obtained for [HOC(O)O$^{\bullet}$·nH$_2$O] with $\underline{n}$ = 1 to 8. That **4H** was a very strong acid was confirmed by the finding that partial ionization spontaneously occurred with only 4 water molecules, and ionization was complete for 5 microsolvating water molecules, i.e., $N_G{}^i$ = 5. The pK_a of **4H** obtained with this computational method (−1.2) was in satisfactory agreement with other estimates (see Scheme 1 and reference [17]). For each of the other radicals in Scheme 1 ($^{\bullet}$XH$_2$WAH), optimized structures were obtained for hydrated clusters ($^{\bullet}$XH$_2$WAH.nH$_2$O) where n was increased until spontaneous dissociation ($^{\bullet}$XH$_2$WA$^-$.nH$_2$O.H$^+$) took place for some value of n (=$N_G{}^i$). Microhydrated cluster structures published by Maity and co-workers for structurally analogous formic [27] and trifluoroacetic acid [28] and by Leopold for various acids [21] served as useful models for the starting points for optimizations. The larger hydration clusters (n > ~8) displayed potential energy surfaces with quite a lot of shallow local minima, such that extensive searching was needed to find the global minima.

2.1. *Microhydration of Carboxyl Radicals* **1Hc** *and* **1Ht**

Carboxyl radicals are important in combustion processes and in the oxidation cycle of Earth's atmosphere because of their formation from the reaction of CO with hydroxyl radicals. The pK_a of **1H** was determined to be −0.2 in a pioneering EPR spectroscopic study by Fessenden and co-workers [29]. The radical's structures and reactions have also been studied experimentally by vibrational [30–32] and rotational spectroscopy [33–35], as well as by a number of high level QM computational methods [36,37]. Experiment and theory indicate that they exist as a pair of *cis*- and *trans*-conformers **1Hc** and **1Ht** separated by a torsional barrier of about 7.7 kcal/mol and with **1Ht** about 1.7 kcal/mol lower in energy [35].

Microhydration of the *cis*-conformer [**1Hc**.nH_2O] was examined for n = 1 to 8 and of the *trans*-conformer **1Ht** for n = 1 to 12. The DFT method with the CAM-B3LYP functional and the 6-311+G(2d,p) basis set (see above) and including the CPCM solvent continuum model was employed.

The PES for each value of n showed a series of minima and the global minimum energy cluster structures were obtained. Figure 1 shows the global minimum energy cluster structures for the *cis*-conformer associated with 1 to 6 H_2O molecules.

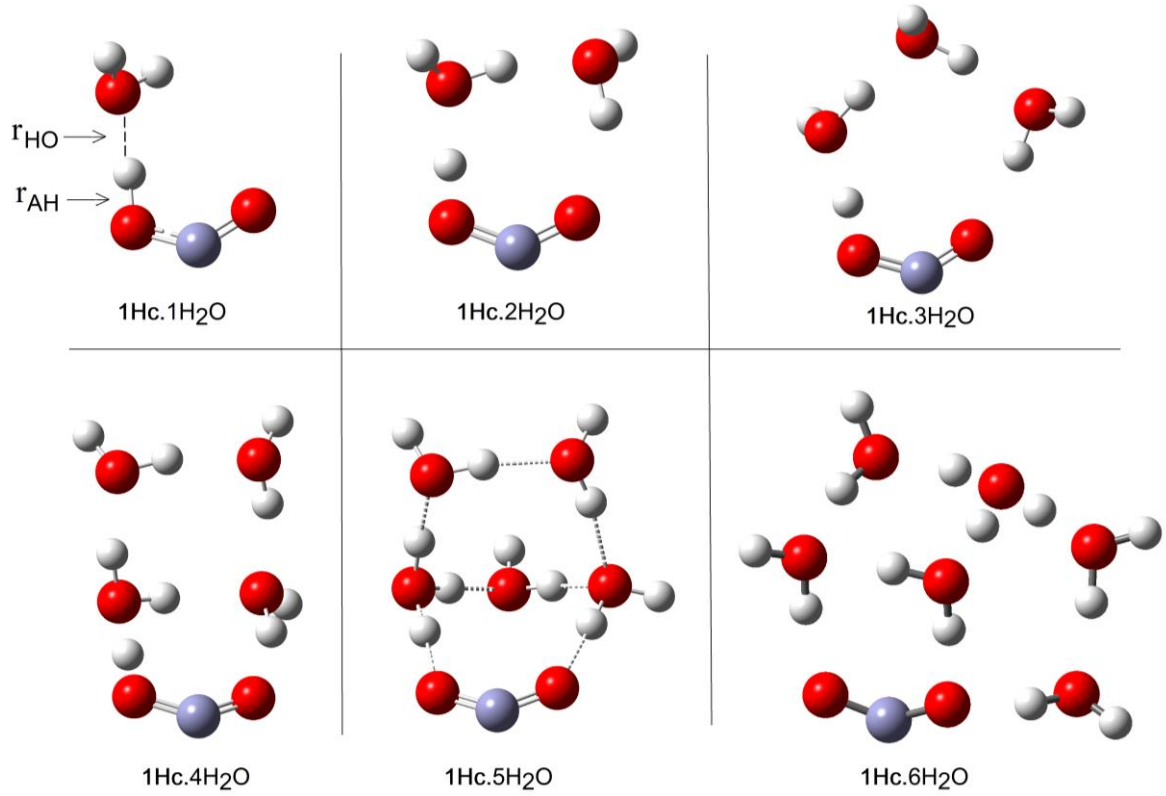

Figure 1. Optimized Cluster Structures of *cis*-Carboxyl (**1Hc**) with 1 to 6 H_2O molecules.

For each value of n (except n = 1), a series of initial structures was tested. Two minima were found for 2 × H_2O clusters, three minima were obtained for 3 × H_2O clusters, and ten were obtained for the 4 × H_2O clusters. In the latter case, several dissociated ion pairs were located as local minima [**1**.H^+ 4H_2O], and one of these was only 4.1 kcal/mol higher in energy than the global undissociated minimum shown in Figure 1. The minimum number of water molecules needed to obtain an ion pair as a local minimum was therefore $N_L{}^i$ = 4. Ten minima were found for the 5 × H_2O cluster and in this case the global minimum structure was an ion pair (Figure 1). Thus, the number of water molecules needed to render the hydrated ion pair [**1**. H^+5H_2O] a global minimum was $N_G{}^i$ = 5. As expected, the number of possible local minima increased steadily with cluster size. For the structures of the global minimum clusters, the computed lengths of the radical acid A–H bonds (OC$^\bullet$O–H), r_{AH}, and the lengths of the bonds from the leaving proton to the nearest H_2O molecule, r_{HO}, (see Figure 1) were useful indicators. These distances are plotted as a function of the number of H_2O molecules in the global minimum clusters for radical **1Hc** in Figure 2. The graph illustrates that r_{AH} remained close to 1.0 Å in the 1× to 4 × H_2O clusters and increased steeply to 1.47 Å in the ionized 5 × H_2O cluster. This behavior was practically mirrored by the distances from the nearest water to the leaving proton (r_{HO}), which remained in the 1.6 to 1.4 Å range for the 1 × to 4 × H_2O clusters before steeply decreasing to 1.04 Å in the 5 × H_2O cluster (see Figure 2).

Hydration of the *trans*-conformer **1Ht** took a rather different course. As with **1Hc,** a series of local minima was obtained for each hydration level. Cluster structures were more open, particularly for mono- to penta-hydration. A significantly higher level of hydration was required to induce ionization.

Global energy minimum structures are illustrated in Figure 3 for selected clusters of **1Ht** with 6 to 11 H_2O molecules.

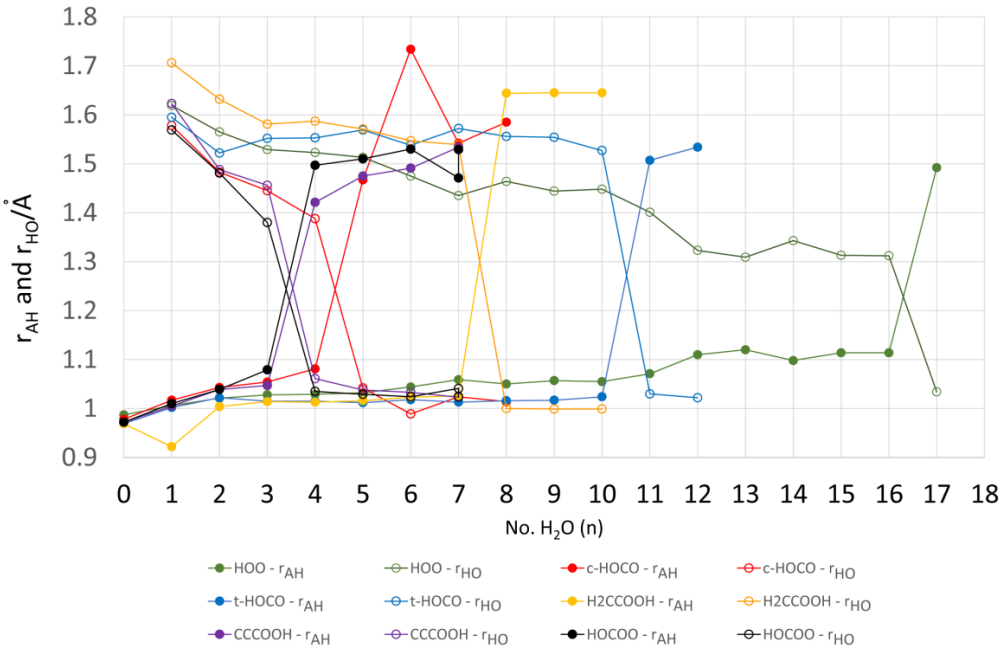

Figure 2. Microhydrated acid radicals (DFT optimized structures): plots of computed distances r_{AH}, and to the nearest water r_{HO}, versus the number of solvating waters (*n*). Data for **4H** (HOCOO, black), **1Ht** (*t*-HOCO, blue), **1Hc** (*c*-HOCO, red), **3H** (H_2CCOOH, yellow), **2H** (CCCOOH, purple), and **5H** (HOO, green).

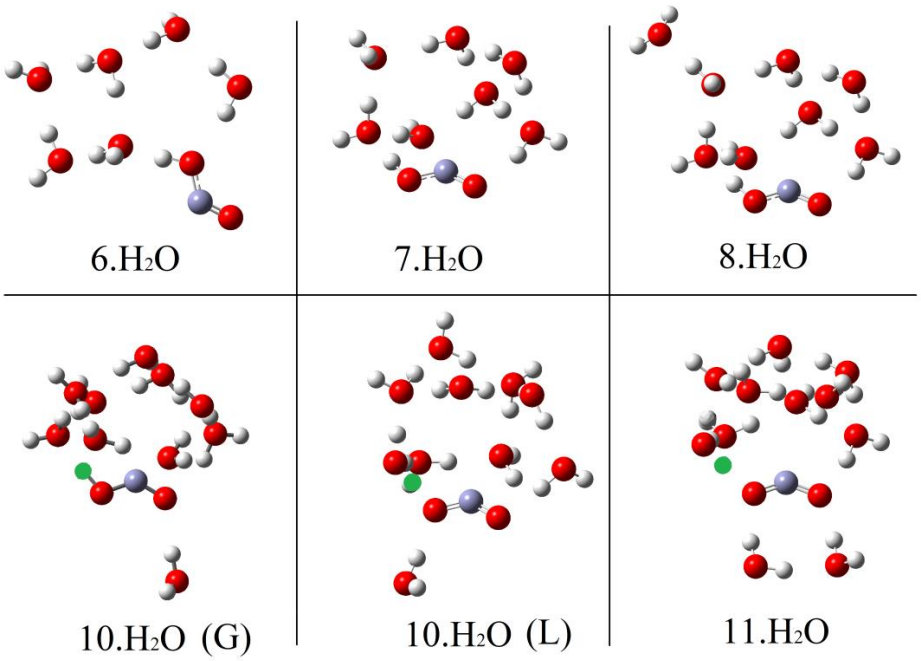

Figure 3. Optimized Cluster Structures of *trans*-Carboxyl (**1Ht**) with 6 to 11 H_2O molecules. Departing proton shown in green.

No clusters containing ionized **1Ht** were obtained for 1× up to 9 × H_2O components. For these clusters, the radical to proton bond length r_{AH} remained steady at about 1.02 Å and the proton to water distance r_{HO} also remained around 1.5 to 1.6 Å (see Figure 2). For 10 microsolvating H_2O molecules, 9 minima were obtained including a local minimum only 2.3 kcal/mol above the global minimum, in which **1Ht** was ionized (see Figure 3 for local and global minima). Finally, with 11 microsolvating H_2O molecules, the global minimum structure contained the fully ionized radical [**1**.11H_2O,H^+] (Figure 3). Thus, for the *trans*-carboxyl radical $N_L{}^i$ = 10 and $N_G{}^i$ = 11.

At first, the much larger $N_G{}^i$ for *trans* **1Ht** than for *cis* **1Hc** seemed surprising. In the case of **1Hc,** the *cis* arrangement of the HO group with the adjacent C–O bond was a crucial feature. This enabled a first water molecule to *H*-bond to this OH and a second water molecule to simultaneously *H*-bond to the first water and to the carboxyl C–O, thus forming a 5-*O*-atom ring (see Figure 1, **1Hc**.2H_2O). Additional waters could then add whilst keeping ring structures intact. Finally, at $N_G{}^i$ = 5, the structure evolved to an ionized 3D cage of rings in which the carboxyl moiety sensed two *H*-bonds and each water sensed at least two (**1Hc**.5H_2O, Figure 1). This arrangement lowered the energy in relation to unionized clusters. With isomer **1Ht**, however, the *trans* arrangement of the H–O group with the adjacent C–O precluded the possibility of two waters simultaneously *H*-bonding to the carboxyl and to each other. A larger, more open ring of waters was needed to stretch from one side of the carboxyl group to the other (see **1Ht**.7H_2O, Figure 3). In fact, the weaker *H*-bonds that resulted meant that four water *H*-bonds to the carboxyl were required before ionization could take place (see **1Ht**.11H_2O, Figure 3).

As mentioned above, **1Ht** is lower in energy than **1Hc** in the gas phase. For the solvated clusters, the difference in DFT computed energies between **1Hc** and **1Ht** [ΔE(c–t)/kcal/mol] are plotted against the number of cage water molecules in Figure 4.

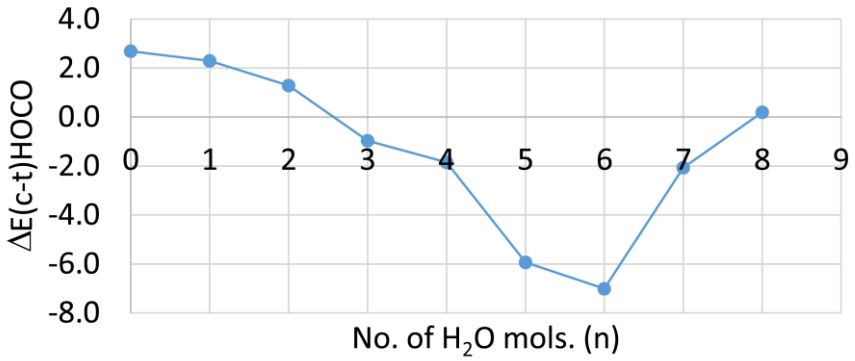

Figure 4. Graph of the Difference in the Energies (kcal/mol) of the **1Hc** and **1Ht** hydrated clusters as a function of the number of cluster water molecules.

It is evident that the *trans*-clusters are lower in energy for 0 to 2 cluster H_2O, but that the *cis*-clusters are lower in energy for 3 to 7 microsolvating H_2O molecules. In aqueous solution, therefore, thermodynamic control should ensure complete deprotonation by five waters. Hence, the experimental pK_a of −0.2 [29] probably corresponds to **1Hc**.

2.2. *Microhydration of Carboxy-ethynyl* **2H** *and Carboxy-methyl* **3H** *Radicals*

The formal structure of the carboxy-ethynyl radical anion **2** (Scheme 1) suggests the upe and charge are separated by the ethyne unit. However, DFT computations predicted **2H** to be a much stronger acid than propiolic acid (HC≡CCO_2H, pK_a = 1.74) and hence to have a sizeable RED-shift [10]. Furthermore, much site exchange of spin and charge was computed for **2** with significant negative charge associated with the terminal ethyne *C*-atom. This was revealed by the Mulliken electronic charges (Figure 5), with the red numbers denoting negative charge. It followed that the normally hydrophobic C≡C unit might, in radical **2H**, take part in *H*-bonding to H_2O, although the electrostatic potential surface (ESP, Figure 5) was fairly featureless, except for the negatively charged (red) *O*-atoms.

It was of special interest therefore to examine microhydration of **2H** to check the prospect of the H_2O clusters extending around to the C≡C terminus, as well as to confirm the enhanced acidity of this species. In the lowest energy structures for clusters with 3 and 4 H_2O molecules (see Figure 5), *H*-bonding took place exclusively in the carboxyl unit. Addition of four H_2O molecules caused spontaneous ionization, and the ionized structure was the global minimum. No ionized minima were found for clusters with only three H_2O molecules and hence $N_L{}^i = N_G{}^i = 4$. This was confirmed by the sudden increase in r_{AH} and decrease in r_{HO} for greater than 4 × H_2O shown on Figure 2. The small $N_L{}^i$ and $N_G{}^i$ agree well with the high predicted acidity (negative pK_a) for **2H**.

The global minimum structure on addition of 5 H_2O molecules was the ionized cage structure shown in Figure 5. However, a unionized structure (Figure 5), obtained simply by expansion of the outer ring of the **2H**.4H_2O cluster, was only 2.6 kcal/mol higher in energy. Another local minimum of the **2H**.5H_2O system did exhibit *H*-bonding to the terminal atom of the ethyne unit as part of a ring connected to a carboxyl *O*-atom (Figure 5). However, this cluster was 10 kcal/mol higher in energy than the global minimum [38]. We deduce that *H*-bonding of H_2O molecules to the ethyne unit of **2H** did not stabilize the conjugate radical anion **2**.

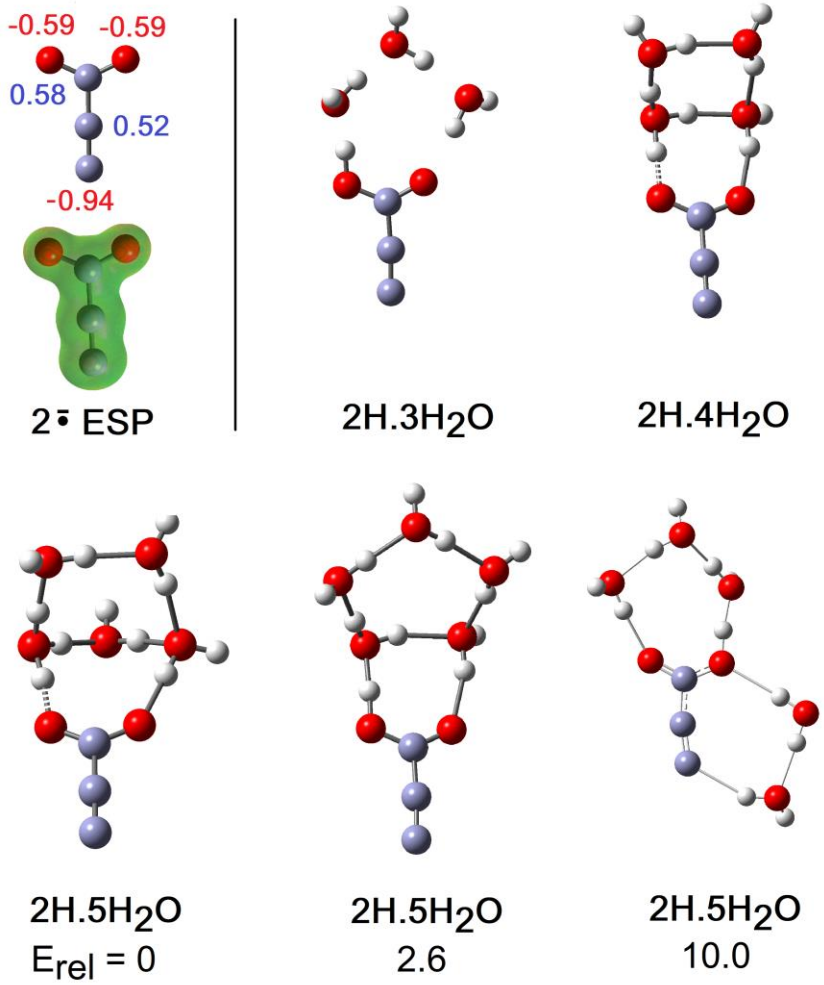

Figure 5. Optimized Structures of Hydration Clusters for Carboxy-ethynyl Radical **2H** and Radical Anion **2**. Mulliken charge: negative in red, positive in blue.

Although the charge and upe in the carboxy-methyl radical **3H** are *formally* separated by only the one *C*-atom of the methylene group, this radical was a much weaker acid than **2H** and comparable in strength to acetic acid. Unlike the ethyne unit, the CH_2 spacer did not transmit any RED-shift to

the carboxyl group. The computational results indicated negative electronic charges associated *only* with the carboxyl *O*-atoms and, in agreement, the ESP surface also showed no negative features adjoining the CH_2 group (see Figure 6). In the cluster for **3H** with only a few H_2O molecules, they *H*-bonded with the carboxyl group and the structures resembled the analogous clusters for **2H,** except that ionization was not observed. Compare, for example, **2H**.4H_2O (ionized) of Figure 5 with **3H**.4H_2O (undissociated) of Figure 6. In striking agreement with the lesser acidity and zero RED-shift of **3H**, ionized structures only appeared as local minima for **3H**.6H_2O (3.6 kcal/mol above the global minimum) and **3H**.7H_2O (1.6 kcal/mol above the global minimum), finally becoming the global minimum for **3H**.8H_2O (see Figure 6). Figure 2 shows the abrupt increase in r_{AH} and abrupt decrease in r_{HO} above 7 × H_2O, and hence it follows that $N_L{}^i$ = 6 and $N_G{}^i$ = 8. Investigations showed large numbers of local minima, differing in energy by < ~6 kcal/mol, for the **3H**.9H_2O, **3H**.10H_2O, **3H**.11H_2O, and **3H**.12H_2O clusters, with some ionized and some undissociated. No clusters involving *H*-bonding to the CH_2 group were found, even with these larger water shells. The elegant optimum structure found for the **3H**.12H_2O cluster (Figure 6) consisted of a symmetrical cage of 5-member *O*-atom rings, atop a planar **3H**.2H_2O unit, forming part of a *quasi*-dodecahedron. The PES could only be partially explored for **3H**.12H_2O, so it is not known if this is a local or global minimum.

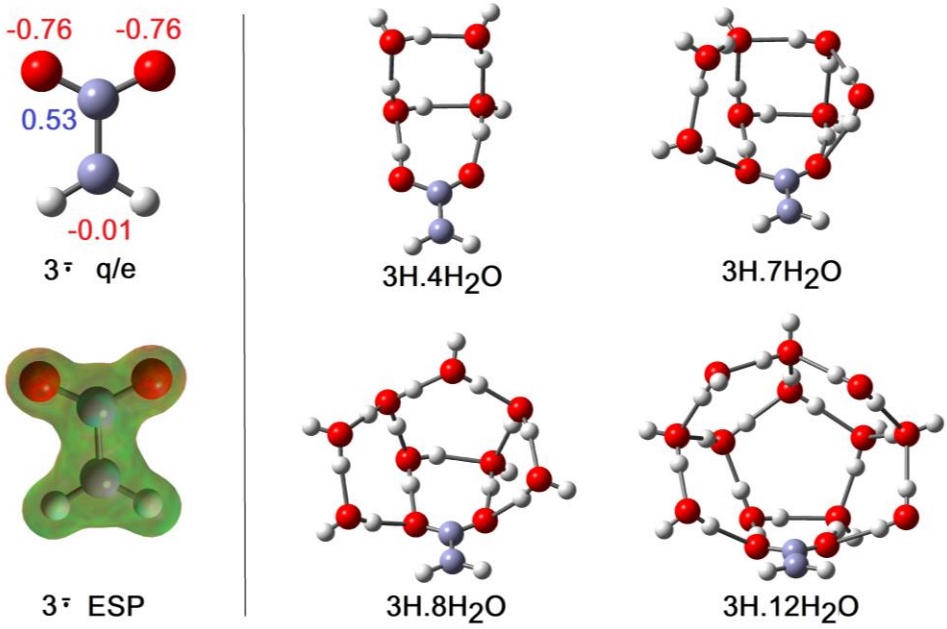

Figure 6. Optimized Structures of Hydration Clusters for Carboxy-methyl Radical **3H** and Radical Anion **3**. Mulliken charges: negative in red, positive in blue.

2.3. *Microhydration of Hydroperoxyl Radicals* **5H**

The hydroperoxyl radical/superoxide radical anion conjugate pair (**5H/5**) has been intensively studied over many years. It plays important roles in lipid peroxidations and in atmospheric chemistry [39–44]. The hydroperoxyl radical differs from the other acid radicals of this study in that it contains two adjacent *O*-atoms rather than the carboxyl unit. It was anticipated, therefore, that the hydrated clusters would have significantly different features. Microhydration of the hydroperoxyl radical **5H** was previously investigated by Novoa and co-workers for *n* = 1–4 and *n* = 10 using the HF/6-31++G(d,p) level of theory [23]. The adsorption and acid dissociation process of **5H** on the surface of $(H_2O)_{20}$ and $(H_2O)_{21}$ clusters were also studied computationally [45]. Not unexpectedly, the CAM-B3LYP/6-311+G(2d,p) method employed here, except for *n* = 1 and 2, gave somewhat different minimum energy structures for hydrated clusters.

The minimum energy cluster structures of **5H**.$n$$H_2O$ were all un-ionized forms for n = 1 to 11; selected examples are in Figure 7 [the r_{AH} and r_{HO} lengths are in Figure 2]. The **5H**.2H_2O structure was similar in essence to analogous carboxy 2×H_2O clusters (above). A noteworthy feature for the 4xH_2O clusters was that structure **5H**.4H_2O(a) containing a 6-*O*-atom ring but only 5 *H*-bonds was lower in energy by 5.4 kcal/mol than structure (**c**) containing 6 *H*-bonds (Figure 7). The three *H*-bonds from waters to the OO unit in structure **5H**.4H_2O(c) are all very long (1.874, 2.079, and 2.431 Å), probably because of angle strain in the two small 4-*O*-rings. In contrast, the *H*-bond from water to the OO unit in structure **5H**.4H_2O(a) is shorter (1.853 Å) and the inter-water *H*-bonds (1.653, 1.712, and 1.737 Å) are considerably shorter than those of **5H**.4H_2O(c). Structure **5H**.4H_2O(b), which contains a 5-*O*-ring, is intermediate in energy, and the inter-water *H*-bonds (1.682, 1.786, 1.857 Å) are also intermediate in length.

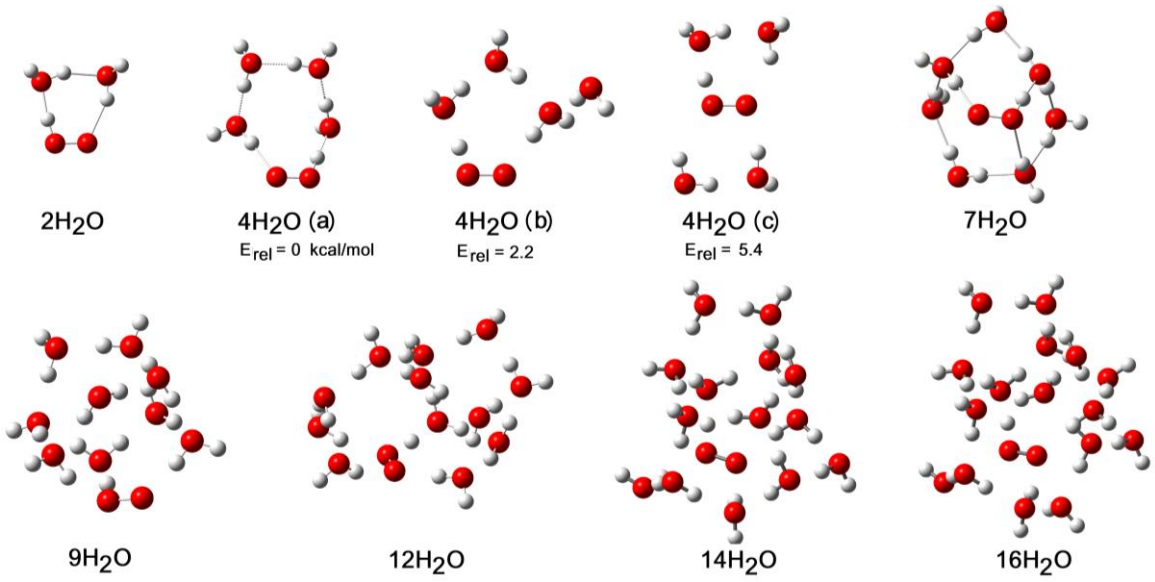

Figure 7. Optimum Structures of Selected HOO• Radical/Water Clusters (**5H**.$n$$H_2O$).

3D cage structures were composed of rings of waters predominated for clusters with 7 or more waters and increased in complexity as more waters were added (see Figure 7). The 3D structures of the **5H**.14H_2O and **5H**.16H_2O clusters contained four H-bonds to the OO unit, and the number of inter-water *H*-bonds tended to a maximum.

The first cage containing ionized $O_2^{-\bullet}$ and H^+ appeared for n = 12, but was 4.3 kcal/mol higher in energy than the undissociated minimum energy structure. It was not possible to exhaustively explore the entire potential energy landscapes for n = 12, 13, 14, 15, and 16. For each of these clusters, both ionized and un-ionized forms were obtained, which differed in energy by < ~10 kcal/mol but with un-ionized cages as energy minima. For the **5H**.17H_2O cluster, 11 local minima were obtained, with 9 being ionized and 2 un-ionized. The lowest energy ionized and un-ionized structures are illustrated in Figure 8. A remarkable result was the smallness of the structural difference that brought about spontaneous dissociation. The relocation of the single water molecule (labelled "a" in Figure 8) from one peripheral site to another was sufficient. This ostensibly minor change, together with concomitant bond length and angle reorganizations, caused a 5 kcal/mol lowering of the energy! $N_L{}^i$ and $N_G{}^i$ were estimated to be 13 and 17, respectively (see Figure 2). However, these larger hydration clusters probably existed as equilibria to which both ionized and un-ionized cages contributed. Under these circumstances, the "number of water molecules needed to induce ionization" ($N_G{}^i$) is probably a fuzzy concept and should probably not be considered as a sharply defined integer. In support of this, note the less abrupt change in the r_{AH} and r_{HO} distances for larger values of n in the **5H**.$n$$H_2O$ clusters as shown in Figure 2.

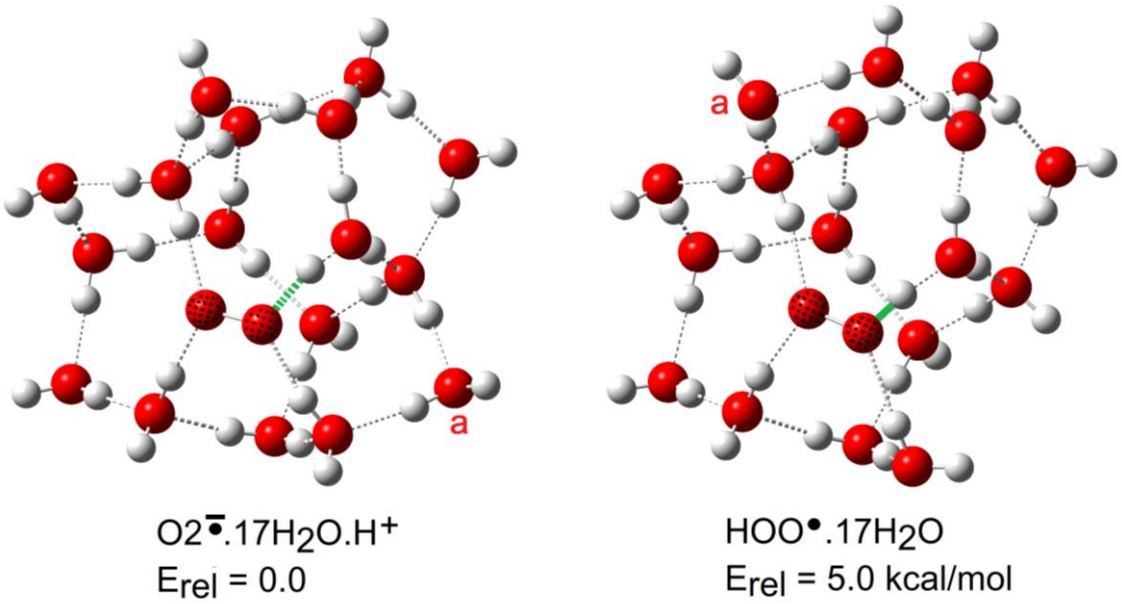

Figure 8. Ionized (left) and un-ionized (right) clusters of the hydroperoxyl radical (**5H**) with 17 H_2O molecules. [Bond to departing H^+ highlighted in green.].

2.4. Microhydration, Acidity, and RED-Shift

The computed numbers of water molecules needed to induce ionization in the radicals $N_G{}^i$ are compared with literature data for mineral acids in Figure 9. Qualitatively, the data make good sense. Radicals **1Hc**, **2H,** and **4H** required only 4 or 5 water molecules to induce deprotonation, i.e., a similar number to acids such as HNO_3 and CF_3COOH. This agrees well with the previous computation of their pK_a values in the same range as mineral acids and gives an independent confirmation of the reality of their RED-shifts.

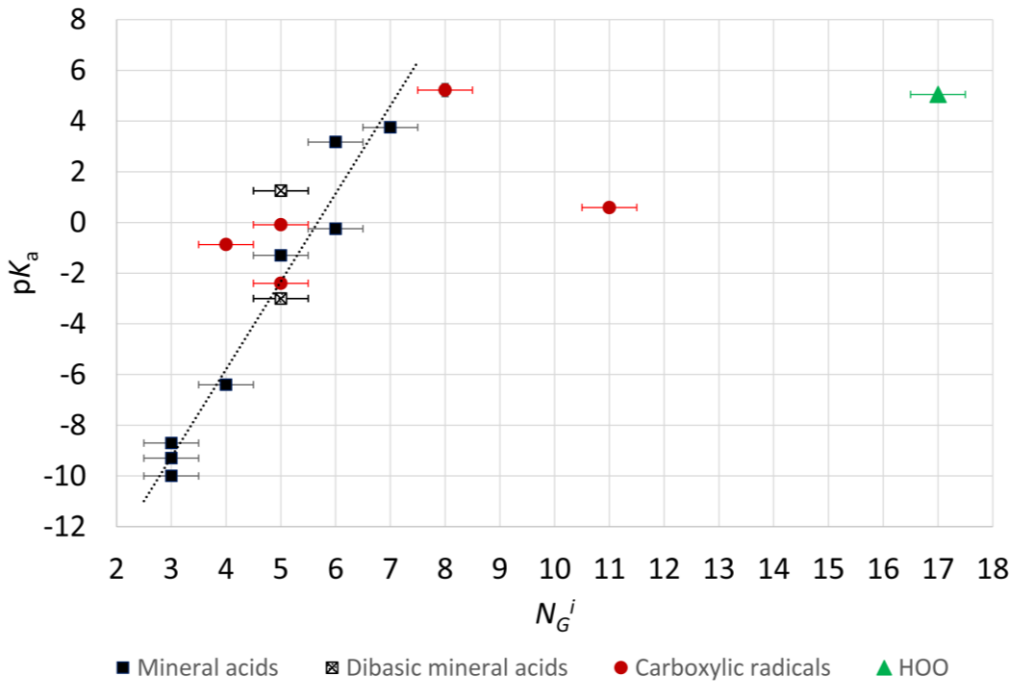

Figure 9. Plots of pK_a versus the number of microsolvating water molecules needed to cause ionization.

The *trans*-carboxyl radical **1Ht** was an obvious outlier and, as explained above, its greater $N_G{}^i$ stems from the somewhat artificial *trans*-structure that, in a real solution, will convert to *cis*. The carboxy-methyl radical **3H** resembled a 'normal' carboxylic acid and needed the same number of water molecules to induce dissociation as formic (and probably acetic) acid. Thus, the microhydration study confirmed the lack of RED-shift for this radical. The data point for the HOO• (**5H**) lies far away from those of the mineral and carboxylate-containing radicals. The radical character of **5H** greatly increases its acidity compared to that of H_2O_2. Structurally, however, the negative charge distributed to two adjacent *O*-atoms of superoxide is much more compact than on the two *O*-atoms of carboxylates. A large cage of water molecules was needed to stabilize this compact conjugate radical anion. That it diverges from the other acid radicals is not at all surprising.

3. Materials and Methods

DFT calculations were carried out using the Gaussian 09 suite of programs [46]. The CAM-B3LYP functional [26] with the 6-311+G(2d,p) basis set was employed for most species with the CPCM continuum model [19] with water as solvent. This model is derived from the COSMO model. Default values of the keywords Alpha, Radii, TSNUM, and TSARE were employed. Based on previous work with free radicals, the CAM-B3LYP functional, which combines the hybrid qualities of B3LYP with the long-range correction proposed by Tawada et al. [47], gave the best results in comparison with G4 (MAD: 2.5 kcal/mol. Functionals of comparable accuracy, such as BMK (MAD 3.2 kcal mol^{-1}), ωB97 (MAD 3.3 kcal mol^{-1}), and M05 (MAD 3.6 kcal mol^{-1}), displayed no significant computational time advantages. Vibrational frequency calculations were implemented so that GS (no imaginary frequencies) and TS status could be checked (one imaginary frequency), and enthalpies and free energies were adjusted for zero point and thermal corrections to 1 atm and 298 K.

4. Conclusions

From this study of the structures of hydrated acid radicals, the following factors that reduced the energy of the hydrated species were identified: (i) *H*-bonding of water to the acidic proton of the radical; (ii) as many *H*-bonds from waters to the *O*-atoms of the radical as possible; (iii) as many *H*-bonds as possible (usually 2 or more) for each water molecule; (iv) rings of *O*-atoms (particularly 5- and 6-membered) were favored over chains or dangling waters for the larger hydrated clusters. The hydration clusters formed primarily round the CO_2 units of the carboxylate-containing radicals and not round either of the CH_2 or C≡C moieties that protruded from the cages. This held true even though the DFT study indicated considerable negative charge associated with the C≡C unit of the carboxy-ethynyl radical **2H**.

Although *trans*-carboxyl (**1Ht**) was lower in energy than **1Hc** in the gas phase, on microhydration the *cis*-clusters became lower in energy after only 3 solvating H_2O molecules. In general, therefore, any carboxylic acid RCO_2H in aqueous solution will probably convert to its *cis*-conformation and ionize from that.

It had previously been predicted that radicals **1Hc**, **2H,** and **4H** would be very strong acids with large RED-shifts [10,18]. The present finding, that just a few water molecules (4 to 5) were sufficient to induce spontaneous ionization of each one, was a valuable, independent corroboration of this. Interestingly, the RED-shift of the carboxy-ethynyl radical **2H** was found not to be due to solvation of its C≡C section. The increased stability of its conjugate radical anion **2** was due to other causes; probably stronger *H*-bonding to the carboxylate. Additionally, essentially zero RED-shift had been predicted for the carboxy-methyl radical **3H**, despite its rather similar structure. The microhydration study was again in full agreement and indicated that many more water molecules (8) were needed to induce ionization of **3H**.

Acknowledgments: The author thanks EaStCHEM for financial support.

Conflicts of Interest: The author declares no conflict of interest. The founding sponsors had no role in the design of the study; in the collection, analyses, or interpretation of data; in the writing of the manuscript; or in the decision to publish the results.

References and Notes

1. Hayon, E.; Simic, M. Acid-base Properties of Free Radicals in Solution. *Acc. Chem. Res.* **1974**, *7*, 114–121. [CrossRef]
2. Steenken, S.; Telo, J.P.; Novais, H.M.; Candeias, L.P. One-electron-reduction Potentials of Pyrimidine Bases, Nucleosides, and Nucleotides in Aqueous Solution. Consequences for DNA redox Chemistry. *J. Am. Chem. Soc.* **1992**, *114*, 4701–4709. [CrossRef]
3. Steenken, S.; Neta, P. One-electron Redox Potentials of Phenols. Hydroxy- and Aminophenols and Related Compounds of Biological Interest. *J. Phys. Chem.* **1982**, *86*, 3661–3667. [CrossRef]
4. Buckel, W.; Keese, R. One-electron Redox Reactions of CoASH Esters in Anaerobic Bacteria—A Mechanistic Proposal. *Angew. Chem. Int. Ed.* **1995**, *34*, 1502–1506. [CrossRef]
5. Smith, D.M.; Buckel, W.; Zipse, H. Deprotonation of Enoxy Radicals: Theoretical Validation of a 50-Year-Old Mechanistic Proposal. *Angew. Chem. Int. Ed.* **2003**, *42*, 1867–1870. [CrossRef] [PubMed]
6. Kim, J.; Darley, D.J.; Buckel, W.; Pierik, A.J. An Allylic Ketyl Radical Intermediate in Clostridial Amino-acid Fermentation. *Nat. Chem.* **2008**, *44*, 239–242. [CrossRef] [PubMed]
7. Studer, A.; Curran, D.P. The Electron is a Catalyst. *Nat. Chem.* **2014**, *50*, 765–773. [CrossRef] [PubMed]
8. Mayer, P.M.; Radom, L. Deprotonating Molecules and Free Radicals to Form Carbon-Centered Anions: A G2 ab Initio Study of Molecular and Free Radical Acidity. *J. Phys. Chem. A* **1998**, *102*, 4918–4924. [CrossRef]
9. Morris, M.; Chan, B.; Radom, L. Effect of Protonation State and Interposed Connector Groups on Bond Dissociation Enthalpies of Alcohols and Related Systems. *J. Phys. Chem. A* **2014**, *118*, 2810–2819. [CrossRef] [PubMed]
10. Walton, J.C. Radical-Enhanced Acidity: Why Bicarbonate, Carboxyl, Hydroperoxyl, and Related Radicals Are So Acidic. *J. Phys. Chem. A* **2017**, *121*, 7761–7767. [CrossRef] [PubMed]
11. Schmidt am Busch, M.; Knapp, E.-W. Accurate pKa Determination for a Heterogeneous Group of Organic Molecules. *ChemPhysChem* **2004**, *5*, 1513–1522. [CrossRef] [PubMed]
12. Silva, C.O.; da Silva, E.C.; Nascimento, M.A.C. Ab initio Calculations of Absolute pKa Values in Aqueous Solution. Part 2. Aliphatic Alcohols, Thiols, and Halogenated Carboxylic Acids. *J. Phys. Chem. A* **2000**, *104*, 2402–2409. [CrossRef]
13. Klicic, J.J.; Freisner, R.A.; Liu, S.-Y.; Guida, W.C. Accurate Prediction of Acidity Constants in Aqueous Solution via Density Functional Theory and Self-Consistent Reaction Field Methods. *J. Phys. Chem. A* **2002**, *106*, 1327–1335. [CrossRef]
14. Klamt, A.; Eckert, F.; Diedenhofen, M.; Beck, M.E. First Principles Calculations of Aqueous pKa Values for Organic and Inorganic Acids Using COSMO-RS Reveal an Inconsistency in the Slope of the pKa Scale. *J. Phys. Chem. A* **2003**, *107*, 9380–9386. [CrossRef] [PubMed]
15. Zhang, S.; Baker, J.; Pulay, P.A. Reliable and Efficient First Principles-Based Method for Predicting pKa Values. 1. Methodology. *J. Phys. Chem. A* **2010**, *114*, 425–431. [CrossRef] [PubMed]
16. Zhang, S.; Baker, J.; Pulay, P.A. Reliable and Efficient First Principles-Based Method for Predicting pKa Values. 2. Organic Acids. *J. Phys. Chem. A* **2010**, *114*, 432–442. [CrossRef] [PubMed]
17. Bühl, M.; DaBell, P.; Manley, D.W.; McCaughan, R.P.; Walton, J.C. Bicarbonate and Alkyl Carbonate Radicals: Structural Integrity and Reactions with Lipid Components. *J. Am. Chem. Soc.* **2015**, *137*, 16153–16162. [CrossRef] [PubMed]
18. Walton, J.C. Enhanced Proton Loss from Neutral Free Radicals: Towards Carbon-Centered Superacids. *J. Phys. Chem. A* **2018**, *122*. [CrossRef] [PubMed]
19. Barone, V.; Cossi, M. Quantum Calculation of Molecular Energies and Energy Gradients in Solution by a Conductor Solvent Model. *J. Phys. Chem. A* **1998**, *102*, 1995–2001. [CrossRef]
20. Gutberlet, A.; Schwaab, G.; Birer, O.; Masia, M.; Kaczmarek, A.; Forbert, H.; Havenith, M.; Marx, D. *Science* **2009**, *324*, 1545–2212. [CrossRef] [PubMed]
21. Leopold, K.R. Hydrated Acid Clusters. *Annu. Rev. Phys. Chem.* **2011**, *62*, 327–349. [CrossRef] [PubMed]

22. Weber, K.H.; Tao, F.M. Ionic Dissociation of Perchloric Acid in Microsolvated Clusters. *J. Phys. Chem. A* **2001**, *105*, 1208–1213. [CrossRef]
23. Del Valle, C.P.; Valdemoro, C.; Novoa, J.J. The Determinant Role of Water in the Ionic Dissociation of HO_2. *J. Mol. Struct. THEOCHEM* **1996**, *371*, 143–152. [CrossRef]
24. Close, D.M.; Wardman, P. Calculation of Standard Reduction Potentials of Amino Acid Radicals and the Effects of Water and Incorporation into Peptides. *J. Phys. Chem. A* **2018**, *122*, 439–445. [CrossRef] [PubMed]
25. Curtiss, L.A.; Redfern, P.C.; Raghavachari, K. Gaussian-4 Theory. *J. Chem. Phys.* **2007**, *126*, 84108–84119. [CrossRef] [PubMed]
26. Yanai, T.; Tew, D.P.; Handy, N.C. A New Hybrid Exchange-correlation Functional Using the Coulomb-attenuating Method (CAM-B3LYP). *Chem. Phys. Lett.* **2004**, *393*, 51–57. [CrossRef]
27. Maity, D.K. How Much Water Is Needed To Ionize Formic Acid? *J. Phys. Chem. A* **2013**, *117*, 8660–8670. [CrossRef] [PubMed]
28. Krishnakumar, P.; Maity, D.K. Effect of microhydration on dissociation of trifluoroacetic acid. *J. Phys. Chem. A* **2014**, *118*, 5443–5453. [CrossRef] [PubMed]
29. Jeevarajan, A.S.; Carmichael, I.; Fessenden, R.W. ESR Measurement of the pKa of Carboxyl Radical and ab initio Calculation of the Carbon-13 Hyperfine Constant. *J. Phys. Chem.* **1990**, *94*, 1372–1376. [CrossRef]
30. Forney, D.; Jacox, M.E.; Thompson, W.E. Infrared Spectra of *trans*-HOCO, $HCOOH^+$, and HCO_2^- Trapped in Solid Neon. *J. Chem. Phys.* **2003**, *119*, 10814–10823. [CrossRef]
31. Johnson, C.J.; Otto, R.; Continetti, R.E. Spectroscopy and Dynamics of the HOCO Radical: Insights into the OH + CO $\rightarrow$ H + CO_2 Reaction. *Phys. Chem. Chem. Phys.* **2014**, *16*, 19091–19105. [CrossRef] [PubMed]
32. Ryazantsev, S.V.; Feldman, V.I.; Khriachtchev, L. Conformational Switching of HOCO Radical: Selective Vibrational Excitation and Hydrogen-Atom Tunneling. *J. Am. Chem. Soc.* **2017**, *139*, 9551–9557. [CrossRef] [PubMed]
33. Radford, H.E.; Wei, W. The rotational spectrum of *trans*-HOCO and DOCO. *J. Chem. Phys.* **1992**, *97*, 3989–3995. [CrossRef]
34. Oyama, T.; Funato, W.; Sumiyoshi, Y.; Endoa, Y. Observation of the Pure Rotational Spectra of *trans*- and *cis*-HOCO. *J. Chem. Phys.* **2011**, *134*, 174303–174307. [CrossRef] [PubMed]
35. McCarthy, M.C.; Martinez, O.; McGuire, B.A.; Crabtree, K.N.; Martin-Drumel, M.-A.; Stanton, J.F. Isotopic Studies of *trans*- and *cis*-HOCO Using Rotational Spectroscopy: Formation, Chemical Bonding, and Molecular Structures. *J. Chem. Phys.* **2016**, *144*, 124304. [CrossRef] [PubMed]
36. Li, Y.; Francisco, J.S. High Level ab initio Studies on the Excited States of HOCO Radical. *J. Chem. Phys.* **2000**, *113*, 7963–7970. [CrossRef]
37. Conte, R.; Houston, P.L.; Bowman, J.M. Communication: A Benchmark-quality, Full-dimensional ab initio Potential Energy Surface for Ar-HOCO. *J. Chem. Phys.* **2014**, *140*, 151101. [CrossRef]
38. As a cross check suggested by a reviewer, structures of the $4\times H_2O$ and $5\times H_2O$ clusters of **2H** were optimized with the CAM-B3LYP-D3/6-311+G(2d,p) method to include Grimme's empirical dispersion corrections. The SMD solvent continuum model was also employed. For each a range of different starting geometries was tried. For both cluster types this method arrived at the same global minimum structures **2H.**$4H_2O$ and **2H.**$5H_2O$ shown in Figure 5. There were some differences in bond lengths and angles. Furthermore, the cluster of the **2H.**$5H_2O$ system exhibiting H-bonding to the terminal atom of the ethyne unit as part of a ring connected to a carboxyl *O*-atom (Figure 5) was again found to be only a local minimum but 7 kcal/mol higher in energy.
39. Bielski, B.H.J.; Cabelli, D.E.; Arudi, R.L.; Ross, A.B. Reactivity of HO_2/O_2^- Radicals in Aqueous Solution. *J. Phys. Chem. Ref. Data* **1985**, *14*, 1041–1100. [CrossRef]
40. Mendes, J.; Zhou, C.-W.; Curran, H.J. Theoretical Chemical Kinetic Study of the H-Atom Abstraction Reactions from Aldehydes and Acids by H Atoms and OH, HO_2, and CH_3 Radicals. *J. Phys. Chem. A* **2014**, *118*, 12089–12104. [CrossRef] [PubMed]
41. Farnia, S.; Vahedpour, M.; Abedi, M.; Farrokhpour, H. Theoretical Study on the Mechanism and Kinetics of Acetaldehyde and Hydroperoxyl Radical: An Important Atmospheric Reaction. *Chem. Phys. Lett.* **2013**, *583*, 190–197. [CrossRef]
42. Iuga, C.; Alvarez-Idaboy, J.R.; Russo, N. Antioxidant Activity of trans-Resveratrol toward Hydroxyl and Hydroperoxyl Radicals: A Quantum Chemical and Computational Kinetics Study. *J. Org. Chem.* **2012**, *77*, 3868–3877. [CrossRef] [PubMed]

43. Espinosa-Garcia, J. Theoretical Study of the Trapping of the OOH Radical by Coenzyme Q. *J. Am. Chem. Soc.* **2004**, *126*, 920–927. [CrossRef] [PubMed]
44. Yin, H.; Xu, L.; Porter, N.A. Free Radical Lipid Peroxidation: Mechanisms and Analysis. *Chem. Rev.* **2011**, *111*, 5944–5972. [CrossRef] [PubMed]
45. Torrent-Sucarrat, M.; Ruiz-Lopez, M.F.; Martins-Costa, M.; Francisco, J.S.; Anglada, J.M. Protonation of Water Clusters Induced by Hydroperoxyl Radical Surface Adsorption. *Chem. Eur. J.* **2011**, *17*, 5076–5085. [CrossRef] [PubMed]
46. Frisch, M.J.; Trucks, G.W.; Schlegel, H.B.; Scuseria, G.E.; Robb, M.A.; Cheeseman, J.R.; Scalmani, G.; Barone, V.; Mennucci, B.; Petersson, G.A.; et al. *Gaussian 09, Revision D.01*; Gaussian, Inc.: Wallingford, CT, USA, 2013.
47. Tawada, Y.; Tsuneda, T.; Yunagisawa, S.; Yanai, T.; Hirao, K. A Long-Range-Corrected Time-Dependent Density Functional Theory. *J. Chem. Phys.* **2004**, *120*, 8425–8433. [CrossRef] [PubMed]

Structure Availability: Cartesian matrices of the optimum clusters are available from the author.